

NMR studies of quantum chaos in a two-qubit kicked top

V R Krithika, V S Anjusha, Udaysinh T. Bhosale, and T. S. Mahesh^{1,*}

¹*Department of Physics and NMR Research Center,
Indian Institute of Science Education and Research, Pune 411008, India*

Quantum chaotic kicked top model is implemented experimentally in a two qubit system comprising of a pair of spin-1/2 nuclei using Nuclear Magnetic Resonance techniques. The essential nonlinear interaction was realized using indirect spin-spin coupling, while the linear kicks were realized using RF pulses. After a variable number of kicks, quantum state tomography was employed to reconstruct the single-qubit density matrices using which we could extract various measures such as von Neumann entropies, Husimi distributions, and Lyapunov exponents. These measures enabled the study of correspondence with classical phase space as well as to probe distinct features of quantum chaos, such as symmetries and temporal periodicity in the two-qubit kicked top.

Keywords: Chaos, kicked top, entanglement, von Neumann entropy

I. INTRODUCTION

Classical chaos is an extensively studied field in physics theoretically and experimentally. Classically chaotic systems are deterministic systems which show sensitivity to initial conditions, rendering the long-time predictions uncertain [1]. Chaos has far-reaching applications not just in physics, but in many diverse fields like biology, chemistry, engineering, etc. [1–3].

The correspondence principle states that classical mechanics is a limiting case of quantum mechanics, in which case, there must be some signatures of chaos in the quantum regime. A direct extension of chaos to quantum mechanics is however not straightforward since (i) quantum dynamics is governed by the Schrödinger equation, which is linear and preserves the overlap of states, and (ii) we can not define trajectories for quantum systems due to the constraint imposed by the uncertainty principle in precisely locating a point in the phase space of the system. A major focus of the field of quantum chaos is to understand the correspondence between quantum and classical evolutions in chaotic systems, and it has been a subject of theoretical as well as experimental interest [4–14].

Study of quantum chaos is not only important from the perspective of understanding fundamental physics, but also for applications in building operable quantum computers since it was shown that the presence of quantum chaos in a system can affect the functionality of a quantum computer [15]. Since classical measures of chaos cannot be extended to the quantum domain, quantum chaos has to be quantified using inherent quantum mechanical properties. Signatures of quantum chaos have been studied using various quantities like entanglement [16–20], Lyapunov exponents and Husimi probability distributions [21], the dynamics of quantum discord [22], level statistics of chaotic Hamiltonians [23, 24], the dynamics of open quantum systems undergoing continuous

quantum measurement [25], etc. The kicked top model is a classic example for studying chaos. It shows regular to chaotic behavior as a function of a parameter, has been studied theoretically [16–19, 23, 26–29], and has been realized experimentally in various systems like laser-cooled cesium atoms [8] and superconducting circuits [11]. Recently, the kicked top consisting of just two qubits, which is in a deep quantum regime, has also been studied theoretically in detail [18, 30]. For two qubits the model is exactly solvable and the same is shown to hold valid for three and four qubits as well [28]. In this work, we investigate quantum chaos in a two-qubit system formed by a pair of spin-1/2 nuclei using Nuclear Magnetic Resonance (NMR) techniques. NMR has been a successful testbed to understand quantum correlations and implement various quantum information processing tasks [31, 32]. NMR offers advantages in terms of long coherence times, precise controllability of quantum dynamics, and efficient measurement of output states. We study quantum kicked top (QKT) using spin-spin interaction between two nuclear spins as the nonlinear evolution and intermittent RF pulses as linear kicks. After a variable number of kicks, we characterize the final state via quantum state tomography (QST). Signatures of the corresponding classical phase space are found in the time averaged von Neumann entropy. Further analysis using Lyapunov exponents and Husimi probability distributions also reveal good classical-quantum correspondence.

The paper is organized as follows. Sec. II introduces the theory of kicked top model. The NMR implementation, results of the experiments, and their analysis along with numerical simulations are presented in Sec. III and final conclusions are given in Sec. IV.

II. QUANTUM KICKED TOP

We now describe using a pair of qubits to simulate a QKT [8, 23] described by the piece-wise Hamiltonian consisting of periodic x -kicks of width Δ and strength p separated by nonlinear evolutions each of an interval

* mahesh.ts@iiserpune.ac.in

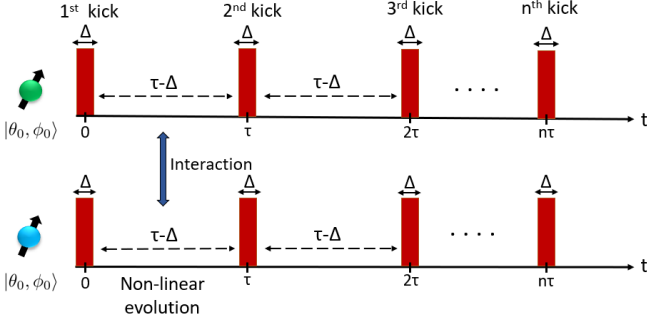


FIG. 1. The linear kicks and nonlinear evolutions for simulating a QKT using two qubits.

$\tau \gg \Delta$ (see Fig. 1)

$$H(t) = p J_x, \text{ for } t \in \left[n\tau - \frac{\Delta}{2}, n\tau + \frac{\Delta}{2} \right] \text{ and,}$$

$$H(t) = \frac{k}{2j\tau} J_z^2 \text{ otherwise.} \quad (1)$$

Here, $\mathbf{J} = [J_x, J_y, J_z]$ is the total angular momentum vector and $[n\tau - \frac{\Delta}{2}, n\tau + \frac{\Delta}{2}]$ describes the time lapse of the n th kick. The value of \hbar has been set to 1. The nonlinear term describes a torsion about the z axis wherein k is the chaoticity parameter. Here, j is the total spin-quantum number. The advantage of this model is that, for a given j it corresponds to $2j$ number of qubits and thus various quantum correlations can be studied [22]. In the case of two-qubits considered here, $j = 1$. Further, we set $p\Delta = \pi/2$ for simplification of the quantum and classical maps [19, 33]. The time evolution is governed by the Floquet unitaries

$$U_{\text{kick}} = e^{-i\frac{\pi}{2}J_x}, U_{\text{NL}} = e^{-i\frac{kJ_z^2}{2j}} \text{ \& } U_{\text{QKT}} = U_{\text{NL}}U_{\text{kick}}. \quad (2)$$

The overall unitary U_{QKT} is applied repeatedly to realize the desired number of kicks. In the Heisenberg picture, the evolution of angular momentum operator for any time step is given by [19]

$$\mathbf{J}' = U_{\text{QKT}}^\dagger \mathbf{J} U_{\text{QKT}}. \quad (3)$$

The x and y components of \mathbf{J} can be recast in the form of raising and lowering operators as $J_x = (J_+ + J_-)/2$ and $J_y = (J_+ - J_-)/2i$ which can then be studied in J_z eigenbasis $\{|m\rangle\}$ following the ladder equations

$$J_+|m\rangle = c_m|m+1\rangle \text{ and } J_-|m\rangle = d_m|m-1\rangle.$$

First let us consider the evolution of J_+ component since J_- will simply be its Hermitian conjugate (H.c):

$$J'_+ = U_{\text{QKT}}^\dagger J_+ U_{\text{QKT}} = U_{\text{kick}}^\dagger U_{\text{NL}}^\dagger J_+ U_{\text{NL}} U_{\text{kick}}. \quad (4)$$

Computing the action of U_{NL} on the operator in $|m\rangle$ ba-

sis,

$$\begin{aligned} \langle m|U_{\text{NL}}^\dagger J_+ U_{\text{NL}}|n\rangle &= \langle m|e^{i\frac{k}{2j}J_z^2} J_+ e^{-i\frac{k}{2j}J_z^2}|n\rangle \\ &= \exp\left\{i\frac{k}{2j}(m^2 - n^2)\right\} \langle m|J_+|n\rangle \\ &= \exp\left\{i\frac{k}{2j}(m^2 - n^2)\right\} c_n \delta_{m,n+1} \\ &= \begin{cases} e^{i\frac{k}{j}(n+\frac{1}{2})} c_n & \text{if } m = n + 1, \\ 0 & \text{otherwise} \end{cases} \\ &= \langle m|J_+ e^{i\frac{k}{j}(J_z + \frac{1}{2})}|n\rangle, \end{aligned} \quad (5)$$

so that

$$U_{\text{NL}}^\dagger J_+ U_{\text{NL}} = J_+ e^{i\frac{k}{j}(J_z + \frac{1}{2})}. \quad (6)$$

Next, the kick Floquet unitary has to be applied on the above operator. The action of kick unitary is to bring about a clockwise rotation about the x axis by an angle of $\pi/2$ giving $U_{\text{kick}}^\dagger (J_x, J_y, J_z) U_{\text{kick}} = (J_x, -J_z, J_y)$, so that

$$\begin{aligned} J'_+ &= U_{\text{QKT}}^\dagger J_+ U_{\text{QKT}} = U_{\text{kick}}^\dagger J_+ e^{i\frac{k}{j}(J_z + \frac{1}{2})} U_{\text{kick}} \\ &= (J_x - iJ_z) e^{i\frac{k}{j}(J_y + \frac{1}{2})}. \end{aligned} \quad (7)$$

The post-iteration transverse components of the angular momentum are thus,

$$\begin{aligned} J'_x &= \frac{J'_+ + J'_-}{2} = \frac{1}{2} \left[(J_x - iJ_z) e^{i\frac{k}{j}(J_y + \frac{1}{2})} + \text{H.c} \right] \text{ and} \\ J'_y &= \frac{J'_+ - J'_-}{2i} = \frac{1}{2i} \left[(J_x - iJ_z) e^{i\frac{k}{j}(J_y + \frac{1}{2})} - \text{H.c} \right]. \end{aligned} \quad (8)$$

For J_z operator, the non-linear Floquet unitary brings about no change since it commutes with J_z . The only evolution of J_z is caused by $\pi/2$ rotation about x axis giving $U_{\text{kick}}^\dagger J_z U_{\text{kick}} = J_y$, so that

$$J'_z = J_y. \quad (9)$$

In the next section, we will study the classical limit of the kicked top.

Classical limit of kicked top

It is insightful to first look into the classical features of the kicked top in the semiclassical limit i.e., $j \rightarrow \infty$. Expressing $X = J_x/j$, $Y = J_y/j$, and $Z = J_z/j$, one obtains $[X, Y] = iZ/j$, which vanishes in the large j limit. Under this classical limit, Eqs. 8 and 9 lead to the iterative map [19, 33]

$$\begin{aligned} X' &= X \cos(kY) + Z \sin(kY) \\ Y' &= X \sin(kY) - Z \cos(kY) \\ Z' &= Y. \end{aligned} \quad (10)$$

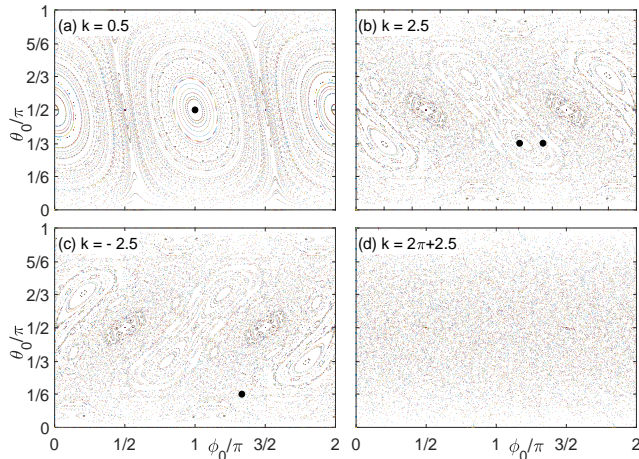


FIG. 2. Classical trajectories of the kicked top in $|\theta, \phi\rangle$ phase space for various values of chaoticity parameter k as indicated. The points chosen for detailed analysis are marked by black dots.

These components can be parametrized in terms of the polar coordinates (θ, ϕ) as $X = \sin\theta \cos\phi$, $Y = \sin\theta \sin\phi$, and $Z = \cos\theta$. As the value of the chaoticity parameter k increases, the phase-space undergoes a transition from a regular to a combination of regular and chaotic regions before becoming predominantly chaotic for large values of k . The classical phase space is shown for different values of k in Fig. 2. The trivial fixed points $(\theta, \phi) = (\pi/2, 0)$ and $(\pi/2, \pi)$ can be seen in Fig. 2(a) which becomes unstable at $k = 2$. At $k = 2$ new fixed points are born and they move away as k is increased as shown in Fig. 2(b). For large value of $k > 5$ the phase-space becomes mostly chaotic as in Fig. 2(d).

In the following we return to the quantum case with a pair of NMR qubits.

III. QKT WITH A PAIR OF NMR QUBITS

Consider a pair of qubits with spin angular-momentum operators \mathbf{I}_1 and \mathbf{I}_2 respectively. By denoting the total z -component $J_z = I_{z1} + I_{z2}$, we obtain the nonlinear term $J_z^2 = 1/4 + 1/4 + 2I_{z1}I_{z2}$. Dropping identities which only introduce global phases, we may realize the nonlinear dynamics using the bilinear term, which naturally occurs in a pair of weakly coupled on-resonant heteronuclear NMR qubits. In a doubly rotating frame, the Hamiltonian is given by

$$H_J = 2\pi J I_{z1} I_{z2}, \quad (11)$$

where J is the indirect spin-spin interaction strength. Comparing the above Hamiltonian with the second term of Eq. 1, we obtain $k = 2\pi J\tau$.

In our experiments, the pair of qubits was formed by ^{19}F and ^{31}P spins of sodium fluorophosphate dissolved in D_2O (5.3 mg in 600 μl). All experiments were performed on a 500 MHz Bruker NMR spectrometer at ambient temperatures and on-resonant conditions.

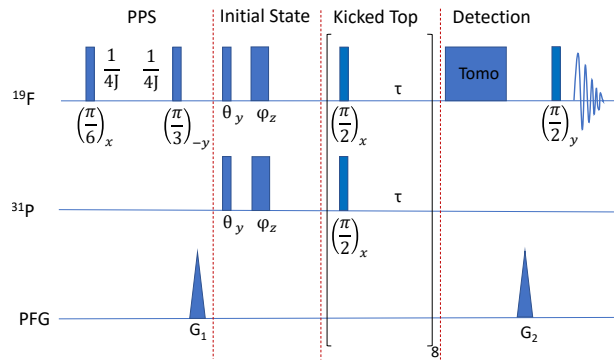


FIG. 3. NMR pulse sequence for simulating a QKT in a two-qubit system. Here G_1 and G_2 correspond to pulsed-field-gradients.

The indirect spin-spin coupling $J = 868$ Hz. The experiments consisted of two parts, i.e., preparation of the initial state (θ_0, ϕ_0) , followed by simulating a QKT as illustrated in Fig. 1.

In NMR systems, owing to the low nuclear polarization at an ambient temperature T and a typical Zeeman field B_0 , the initial thermal equilibrium state

$$\rho_0 = \frac{1}{4} + \frac{\epsilon}{2}\tilde{\rho}.$$

is highly mixed with the low purity factor $\epsilon \sim 10^{-5}$. The uniform background population represented by identity remains invariant under the unitary evolution, while the traceless deviation density matrix $\tilde{\rho} = I_{z1} + I_{z2}$ evolves and captures all the interesting dynamics.

In the following we utilize $\{|0\rangle, |1\rangle\}$ eigenbasis of I_z as the computational basis. We first prepare the $|00\rangle$ pseudopure state (PPS) by transforming $\tilde{\rho}$ into $I_{z1} + I_{z2} + 2I_{z1}I_{z2}$ using a pair of pulses followed by a pulsed field gradient (PFG) as shown in Fig. III [34].

Subsequently, a θ_y rotation followed by a ϕ_z rotation as shown in Fig. III initialize each of the qubits along a spin coherent state,

$$|\theta, \phi\rangle = \cos(\theta/2)|0\rangle + e^{i\phi}\sin(\theta/2)|1\rangle, \quad (12)$$

on the Bloch sphere, analogous to the classical case. The latter pulses for different ϕ angles were generated by an optimal control technique [35]. The resulting state is

$$\rho_{\theta, \phi} \approx \left(1 - \frac{\epsilon}{2}\right) \frac{1}{4} + \frac{\epsilon}{2} |\theta, \phi\rangle\langle\theta, \phi|. \quad (13)$$

We now apply kicks via radio-frequency $(\pi/2)_x$ pulses with Hamiltonian

$$H_{\text{rf}} = \frac{\pi}{2\Delta}(I_{x1} + I_{x2}), \quad (14)$$

where the pulse duration $\Delta \ll \tau = k/(2\pi J)$, the dura-

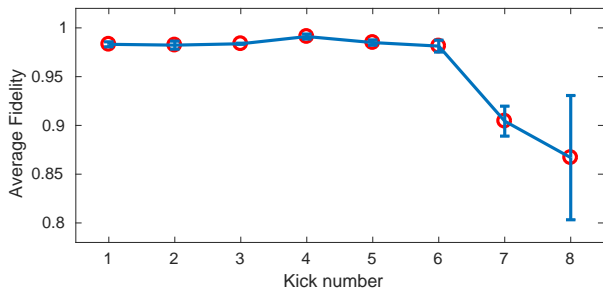


FIG. 4. Average fidelity of the experimental states for various kick-numbers. The errorbars indicate one standard deviation of distribution.

tion of nonlinear evolution corresponding to the chaoticity parameter k (see Fig.1). Thus in our experiment, $U_{\text{kick}} = \exp(-iH_{\text{IF}}\Delta)$, $U_{\text{NL}} = \exp(-iH_{\text{J}}\tau)$, and $U_{\text{QKT}} = U_{\text{NL}}U_{\text{kick}}$ (see Eq. 2)

We applied U_{QKT} for up to n times and estimated the ^{19}F reduced density operator $\rho_n = \text{Tr}_{\text{P}} [U_{\text{QKT}}^n \rho_{\theta, \phi} U_{\text{QKT}}^{\dagger n}]$ using single-qubit pure-phase QST. It consists of following three NMR experiments: (i) A PFG to destroy all the coherences followed by $(\pi/2)_y$ pulse to obtain the diagonal elements; (ii) $(\pi/2)_{-y}$ pulse followed by a PFG and $(\pi/2)_y$ pulse to obtain real part of off-diagonal coherence element; (iii) $(\pi/2)_{-x}$ pulse followed by PFG and $(\pi/2)_y$ pulse to obtain the imaginary part of the off-diagonal coherence element. This way one obtains a pure-phase NMR signal which can be easily quantified without any further numerical processing. We estimated the fidelity

$$F(\tilde{\rho}_n, \tilde{\rho}_n^{\text{th}}) = \frac{\text{Tr} [\tilde{\rho}_n \tilde{\rho}_n^{\text{th}}]}{\sqrt{\text{Tr} [\tilde{\rho}_n^2] \text{Tr} [(\tilde{\rho}_n^{\text{th}})^2]}} \quad (15)$$

of the experimental deviation state $\tilde{\rho}_n$ with the theoretical deviation state $\tilde{\rho}_n^{\text{th}}$ for all initialization points (θ, ϕ) and for all k values. The average fidelity versus kick number displayed in Fig. 4 indicates high fidelities of above 0.95 upto six kicks and above 0.8 upto 8 kicks.

A. Probing quantum chaos via von Neumann entropy

It has been observed that a kicked top in a state corresponding to a classically chaotic region results in a higher entanglement production [19]. Since the degree of entanglement can be quantified by the von Neumann entropy

$$S(\rho_n) = - \sum_{\lambda_{\pm} \neq 0} \lambda_{\pm} \log_2 \lambda_{\pm} \quad (16)$$

of the reduced density operator ρ_n with eigenvalues $\lambda_{\pm} = (1 \pm \epsilon\alpha)/2$ where $\pm\alpha$ are eigenvalues of the traceless deviation part. Since in low purity conditions, the von Neu-

mann entropy is close to unity and displays very low contrast between regular and chaotic regions, we define an n^{th} -kick order parameter

$$s_n = \frac{1 - \frac{1}{n} \sum_{m=1}^n S(\rho_m)}{\epsilon^2} \quad (17)$$

which extracts information from the deviation part and hence is a convenient measure of chaos.

We carried out four sets of experiments for chaoticity parameter $k \in \{0.5, 2.5, 2\pi - 2.5, 2\pi + 2.5\}$. In each case, we performed experimental QST and estimated the order parameter s_n for the number n of kicks ranging from 1 to 8. The contours in Fig. 5 display the experimental order parameter s_n for various values of n as well as k . The color background is provided to compare the experimental contours with numerically simulated values of order parameter. In each case, we have also calculated the root-mean-square (RMS) deviation δ between the experimental and the simulated values. There appears to be a general agreement between the experimental and the simulated values.

For one kick at $k = 0.5$ we observe almost uniformly high order parameter $s > 0.6$, while for other k values, we observe similar patterns with a pair of highly ordered regular islands. Gradually, with larger number of kicks, the order parameter settles to a characteristic pattern that resembles the classical phase-space except for $k = 2\pi + 2.5$. Ultimately, we see domains of regular islands corresponding to high order parameter for all k values. As expected, we observe overall high order parameter for the lowest k value. On the other hand, for high k values, unlike the classical case which shows highly chaotic phase-space, in the quantum scenario, the regular islands survive. This is due to the periodicity of the order parameter w.r.t. chaoticity parameter, i.e., $s(k) = s(\text{mod}(k, 2\pi))$. This is evident from the similarity between the contours of column 2 and 4 in Fig. 5 as well as from the reflection symmetry between the columns 2 (or 4) and 3. The periodicity of entropy distribution as a function of chaoticity parameter k and the number of qubits has been theoretically studied in detail in [30].

B. Husimi probability distribution

Although the von Neumann entropy captures the mixedness of the reduced density operator, it is not sensitive to its angular location on the Bloch sphere. The Husimi probability function measures overlap of the state ρ_n at any time with Bloch vectors $\{|\theta, \phi\rangle\}$ on the phase space and is given by

$$Q_n(\theta, \phi, t) = \frac{1}{\pi} \langle \theta, \phi | \rho_n | \theta, \phi \rangle \quad (18)$$

While states initialized to regular regions are expected to be localized at all times, those initialized at other regions explore more of the Bloch sphere. Higher the degree of

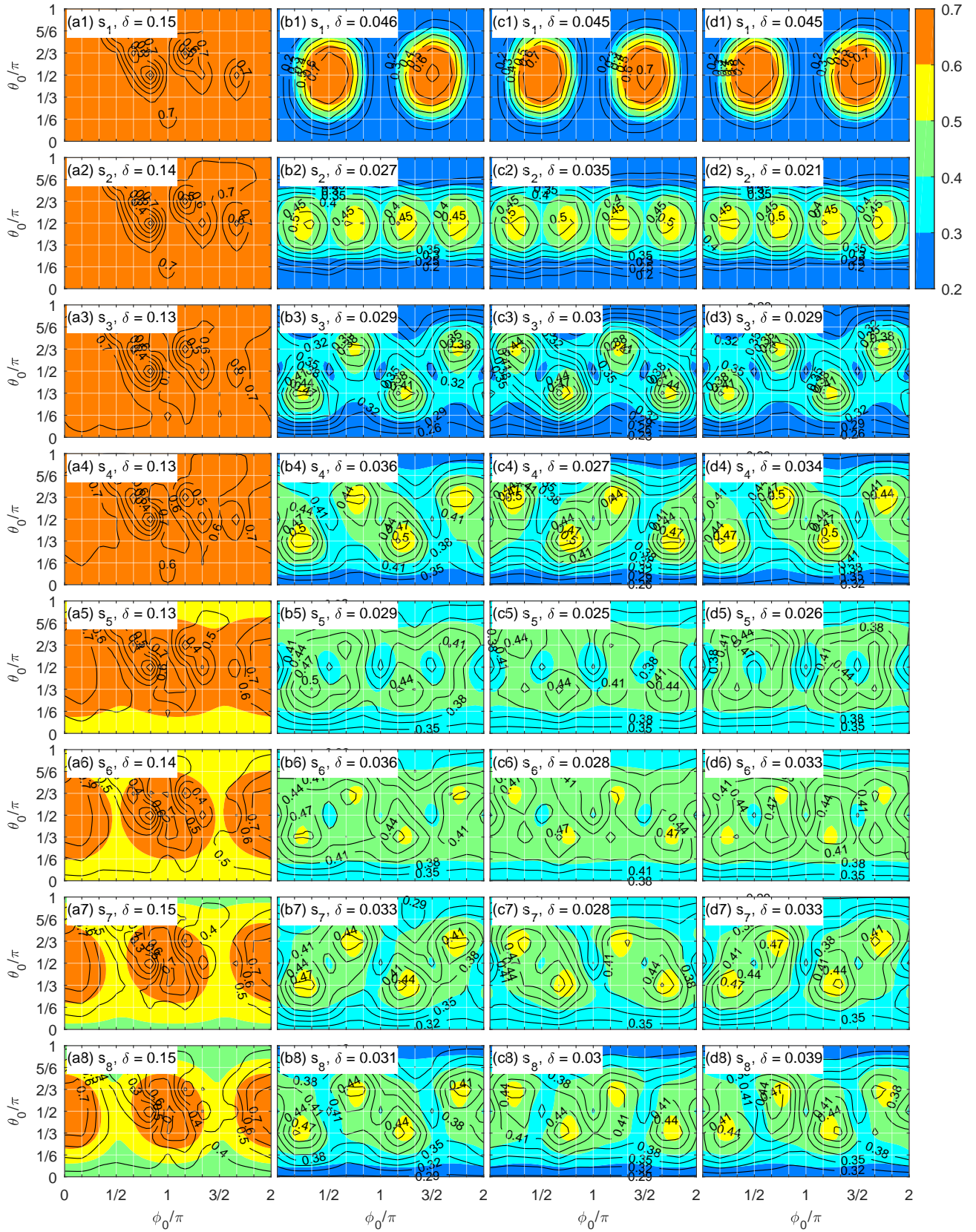


FIG. 5. Contours represent experimental order parameter averaged over n -kicks (s_n) for chaoticity parameter $k = 0.5$ (a1 to a8), $k = 2.5$ (b1 to b8), $k = 2\pi - 2.5$ (c1 to c8), and $k = 2\pi + 2.5$ (d1 to d8). Background colormaps represent the corresponding simulated values. RMS deviations (δ) between the experimental and simulated values are shown in each case.

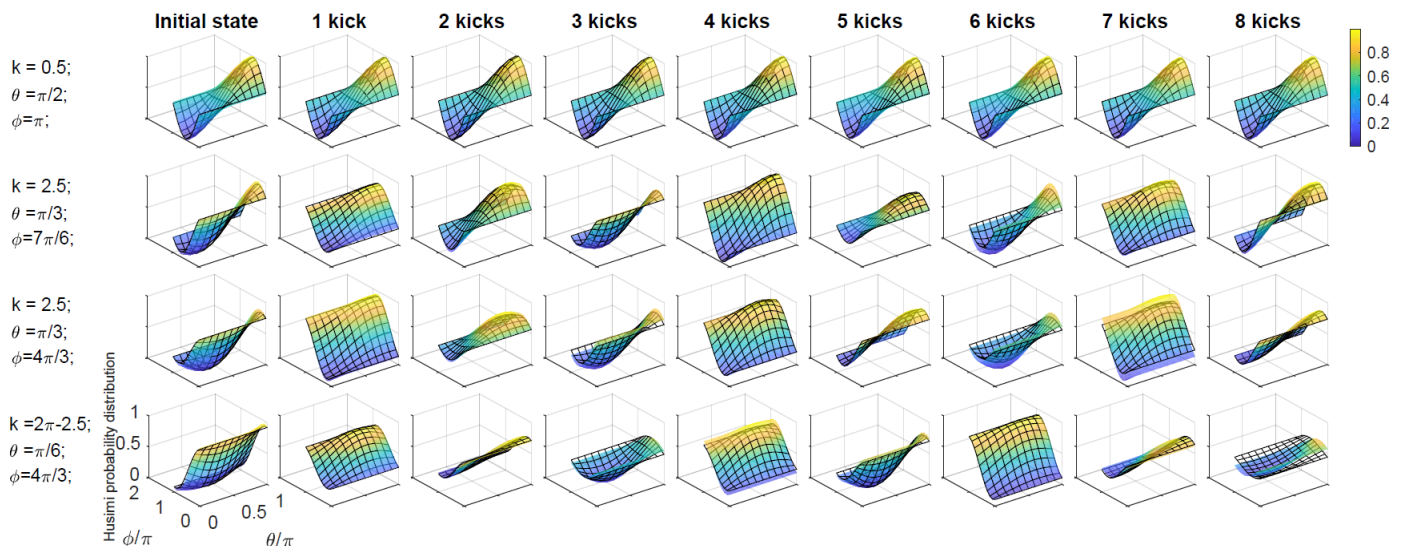


FIG. 6. Experimental (mesh-grids) and simulated (color background) Husimi probability distributions (in units of $1/\pi$) for certain k values and initial states (as marked in Fig. 2) for various number of kicks.

chaos, more is the spreading of the state. The Husimi distributions for select values of k and initial states are shown in Fig. 6. Here the mesh-grid lines represent the experimental distribution while the colour background represents the numerically simulated distribution. We see that the state $|\pi/2, \pi\rangle$ for $k = 0.5$ which lies in the high order-parameter region is localized throughout the evolution time. On the other hand states initialized to lower order-parameter regions undergo periodic temporal modulations and thus exhibit significant delocalization over the Bloch sphere.

To capture the delocalization better, we tracked the dynamics of the first twenty maxima of the Husimi prob-

ability distribution. As shown in Fig. 7, the maxima region for $k = 0.5$ are localized after the evolution, whereas for higher values of k , the maxima regions spread out on the phase space. Interestingly, the mismatch between experiment and simulated data increases with increasing k , implying the sensitivity of the system dynamics to initial conditions and experimental imperfections.

C. Lyapunov exponents

The Lyapunov exponent is a measure of chaos that determines whether the trajectories of two initially very close points diverge or converge over time. In the classical phase space, the Euclidean distance is usually used as the distance measure. For nearby quantum initial states $\rho_0^{(1)}$ and $\rho_0^{(2)}$, we may instead use the fidelity measure $d_m = 1 - F(\rho_m^{(1)}, \rho_m^{(2)})$ (see Eq. 15) to characterize the distance after m kicks. The discrete time Lyapunov exponent after n kicks is defined as

$$\lambda(n) = \frac{1}{n} \sum_{m=1}^n \log \frac{d_m}{d_{m-1}}, \quad (19)$$

and its asymptotic limit $\lim_{n \rightarrow \infty} \lambda(n)$ being positive is considered as a witness for chaoticity. A system initialized in a regular region is characterized by a negative Lyapunov exponent and therefore a pair of nearby trajectories ultimately converge. On the other hand, trajectories of a pair of nearby initial states corresponding to a positive Lyapunov exponent diverge over time, and hence lead to a chaotic behavior. Fig. 8 displays experimentally extracted Lyapunov exponents for certain pairs of nearby initial states after various number of kicks. For compar-

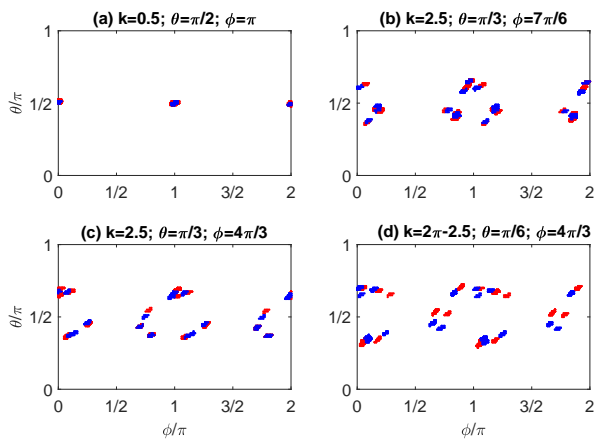


FIG. 7. Distribution of maxima neighborhood of Husimi probability function on the Bloch sphere. Blue dots represent simulated data and red dots represent experimental data for the values of k and initial angles mentioned therein.

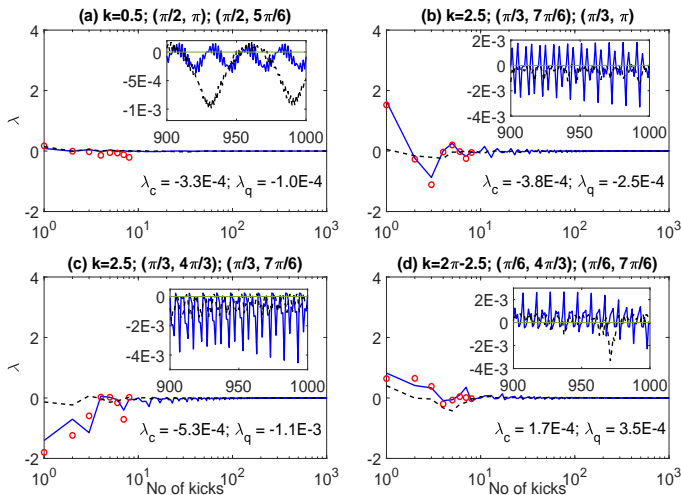


FIG. 8. Experimental Lyapunov exponents for up to 8 kicks for certain k values and pairs of initial states (mentioned in the titles) are shown by red circles. The simulated Lyapunov exponents with classical dynamics (black dashed line) and with quantum dynamics (blue solid line) for up to 1000 kicks are shown for comparison. Means of the last 100 simulated exponents (zoomed in the insets) are also mentioned for classical (λ_c) as well as quantum (λ_q) cases to understand the asymptotic behavior.

son, we have also plotted simulated Lyapunov exponents for the corresponding classical as well as quantum dynamics for up to 1000 kicks which help us to evaluate the asymptotic behavior. The last 100 exponents in each case are zoomed in the insets. The discrete time Lyapunov exponents in Fig. 8(a), which corresponds to the most ordered region, remain close to zero at all times, and slowly converge to a negative value. The means λ_c and λ_q of the last 100 classical and quantum exponents respectively, are also negative indicating the regular dynamics. Although Lyapunov exponents of Fig. 8 (b) and (c) show relatively large fluctuations, they too converge towards zero over larger number of kicks. It can be seen that for Fig. 8(a), (b), and (c), which correspond to regular regions (see Fig. 2), both classical and quantum exponents are predominantly negative and accordingly their respective means λ_c and λ_q also are negative. However, for Fig. 8(d) which corresponds to a chaotic region (see Fig. 2), both classical and quantum exponents are predominantly positive as reflected in their positive means.

IV. CONCLUSIONS

In this work, we have experimentally studied quantum signatures of classical chaos on a two-qubit NMR system

using a kicked top model. We characterized the dynamics via three distinct ways:

(i) Correspondence to classical phase-space was studied using order-parameter profiles extracted from the von-Neumann entropy. These profiles not only showed a good correspondence with the classical phase-space for lower chaoticity parameters, but also showed the inherent periodicity and symmetry in the quantum dynamics for larger values of the chaoticity parameter. It is interesting to see such signatures in the NMR case where the quantum state purity is well below the threshold for entanglement.

(ii) The localization/delocalization of the quantum states on the Bloch sphere was characterized via Husimi probability distribution. They also showed temporal periodicity that is characteristic of the quantum system. We observed the localization of the profiles for low chaoticity conditions and significant delocalization otherwise. In addition, it also highlighted the sensitivity of the distribution to experimental imperfections particularly at higher values of chaoticity parameter.

(iii) Finally we characterized the asymptotic behavior of the nearby trajectories via Lyapunov exponents. The experimentally extracted discrete time exponents gradually decayed towards zero. However, those corresponding to highly periodic region settled to negative values clearly indicating non-chaotic behavior. The simulated exponents for large number of kicks could clearly distinguish the periodic region from the chaotic region.

The system considered here, being only two qubits, is deeply embedded in the quantum regime, but the marks of quantum chaos are nonetheless interesting. NMR testbed should facilitate the possibility of extending such studies with higher number of qubits. Further investigation of other quantum correlation measures such as discord, negativity, etc. will help better understand the bridge between chaos in classical and quantum systems.

ACKNOWLEDGMENTS

We acknowledge useful discussions with Prof. Santhanam, Sudheer Kumar, Deepak Khurana, and Soham Pal. This work was partly supported by DST/SJF/PSA-03/2012-13 and CSIR 03(1345)/16/EMR-II. UTB acknowledges the funding received from Department of Science and Technology, India under the scheme Science and Engineering Research Board (SERB) National Post Doctoral Fellowship (NPDF) file Number PDF/2015/00050.

[1] E. Ott, *Chaos in Dynamical Systems* (Cambridge University Press, Cambridge, UK, 2002).

[2] S. Strogatz, *Nonlinear Dynamics and Chaos* (Perseus Publishing, 2000).

- [3] T. Kapitaniak, *Chaos for Engineers: Theory, Applications, and Control* (Springer-Verlag Berlin Heidelberg, 2000).
- [4] S. Tomsovic and D. Ullmo, Phys. Rev. E **50**, 145 (1994).
- [5] W. K. Hensinger, H. Haffner, A. Browaeys, N. R. Heckenberg, K. Helmerson, C. McKenzie, G. J. Milburn, W. D. Phillips, S. L. Rolston, H. Rubinsztein-Dunlop, and B. Upcroft, Nature (London) **412**, 52 (2001).
- [6] D. A. Steck, W. H. Oskay, and M. G. Raizen, Science **293**, 274 (2001).
- [7] T. Graß, B. Juliá-Díaz, M. Kuś, and M. Lewenstein, Phys. Rev. Lett. **111**, 090404 (2013).
- [8] S. Chaudhury, A. Smith, B. E. Anderson, S. Ghose, and P. S. Jessen, Nature **461**, 768 (2009).
- [9] G. B. Lemos, R. M. Gomes, S. P. Walborn, P. H. S. Ribeiro, and F. Toscano, Nat. Commun. **3**, 1211 (2012).
- [10] J. Larson, B. M. Anderson, and A. Altland, Phys. Rev. A **87**, 013624 (2013).
- [11] C. Neill, P. Roushan, M. Fang, Y. Chen, M. Kolodrubetz, Z. Chen, A. Megrant, R. Barends, B. Campbell, B. Chiaro, *et al.*, Nature Physics (2016).
- [12] M. Bitter and V. Milner, Phys. Rev. Lett. **118**, 034101 (2017).
- [13] E. V. H. Doggen, B. Georgeot, and G. Lemarié, Phys. Rev. E **96**, 040201 (2017).
- [14] D. Wintgen and H. Friedrich, Phys. Rev. Lett. **57**, 571 (1986).
- [15] B. Georgeot and D. L. Shepelyansky, Phys. Rev. E **62**, 6366 (2000).
- [16] X. Wang, S. Ghose, B. C. Sanders, and B. Hu, Phys. Rev. E **70**, 016217 (2004).
- [17] M. Lombardi and A. Matzkin, Phys. Rev. E **83**, 016207 (2011).
- [18] J. B. Ruebeck, J. Lin, and A. K. Pattanayak, Phys. Rev. E **95**, 062222 (2017).
- [19] J. N. Bandyopadhyay and A. Lakshminarayan, Phys. Rev. E **69**, 016201 (2004).
- [20] J. N. Bandyopadhyay and A. Lakshminarayan, Phys. Rev. Lett. **89**, 060402 (2002).
- [21] F. Haake, H. Wiedemann, and K. Zyczkowski, Ann. Physik **1**, 531 (1992).
- [22] V. Madhok, V. Gupta, D.-A. Trottier, and S. Ghose, Phys. Rev. E **91**, 032906 (2015).
- [23] F. Haake, *Quantum Signatures of Chaos* (Springer, 3rd Edition, Berlin, 2010).
- [24] O. Bohigas, M. J. Giannoni, and C. Schmit, Phys. Rev. Lett. **52**, 1 (1984).
- [25] T. Bhattacharya, S. Habib, and K. Jacobs, Phys. Rev. Lett. **85**, 4852 (2000).
- [26] U. T. Bhosale and M. S. Santhanam, Phys. Rev. E **95**, 012216 (2017).
- [27] M. Kumari and S. Ghose, Phys. Rev. E **97**, 052209 (2018).
- [28] S. Dogra, V. Madhok, and A. Lakshminarayan, arXiv preprint arXiv:1808.07741 (2018).
- [29] M. Kumari and S. Ghose, arXiv preprint arXiv:1806.10545 (2018).
- [30] U. T. Bhosale and M. Santhanam, arXiv preprint arXiv:1806.06184 (2018).
- [31] D.G.Cory, R. Laflamme, E. Knill, and et al., Fortschr. Phys. **48 9-11**, 875 (2000).
- [32] I. S. Oliveira, T. J. Bonagamba, R. S. Sarthour, J. C. Freitas, and E. R. deAzevedo, *NMR Quantum Information Processing* (Elsevier Science, The Netherlands, 2007).
- [33] F. Haake, M. Kus, and R. Scharf, Z. Phys. B **65**, 381 (1987).
- [34] D. G. Cory, A. F. Fahmy, and T. F. Havel, Proc. Natl. Acad. Sci., USA **94**, 1634 (1997).
- [35] N. Khaneja, T. Reiss, C. Kehlet, and et. al., Journal of Magnetic Resonance **172**, 296 (2005).